

# Characterization of layered silicate HUS-5 and formation of novel nanoporous silica through transformation of HUS-5 ion-exchanged with alkylammonium cations†

Cite this: *J. Mater. Chem. A*, 2013, **1**, 9680

Nao Tsunoji,<sup>a</sup> Miki Fukuda,<sup>a</sup> Kaname Yoshida,<sup>b</sup> Yukichi Sasaki,<sup>b</sup> Takuji Ikeda,<sup>c</sup> Yusuke Ide,<sup>d</sup> Masahiro Sadakane<sup>a</sup> and Tsuneji Sano<sup>\*a</sup>

Hiroshima University Silicate-1 (HUS-1) and its precursor (HUS-5), whose crystal structure was similar to that of  $\beta$ -HLS layered silicate, were prepared. The interlayer distance of HUS-5 was 0.4 nm; both  $\text{Na}^+$  cations and hydrated water were present in the interlayer. The interlayer distance of HUS-5 was expanded by ion-exchanging with several bulky organic cations such as dodecyltrimethylammonium, hexadecyltrimethylammonium, and benzyltrimethylammonium. The HUS-5 variants that were ion-exchanged with alkylammonium exhibited high catalytic activities base catalysts in a Knoevenagel condensation reaction. In particular, the HUS-5 that was ion-exchanged with hexadecyltrimethylammonium cations was converted to novel nanoporous silica by acetic acid treatment and subsequent calcination and was named HUS-6. The BET surface area and average pore diameter were  $983 \text{ m}^2 \text{ g}^{-1}$  and 1.6 nm, respectively. Formation of nanopores in HUS-6 was clearly confirmed by TEM. Nanopores (ca. 1.6 nm) of HUS-6 present a unique adsorption space; there was an intermediate state between micropores (ca. 0.6 nm) of silicalite-1 and mesopores (ca. 2.9 nm) of MCM-41.

Received 19th May 2013

Accepted 25th June 2013

DOI: 10.1039/c3ta11971h

[www.rsc.org/MaterialsA](http://www.rsc.org/MaterialsA)

## Introduction

Frameworks of crystalline layered silicates (CLSs) are composed exclusively of  $\text{SiO}_4$  tetrahedra. Because reactive  $\text{SiOH}/\text{SiO}^-$  groups are located on the interlayer surface, the layered silicate is easily functionalized by various modification methods such as cation exchange, silylation, and pillaring. CLSs are used in many applications such as catalysts and adsorbents.<sup>1,2</sup> They can also be deployed in the synthesis of porous materials such as zeolite and mesoporous silica.<sup>3-5</sup> In the case of zeolite synthesis, transformation of a layered silicate into zeolite is called topotactic conversion. Here, the silanol groups on the interlayer surfaces of the layered silicates are condensed between the layers, and the layered structures are transformed into zeolite-like 3D structures. If the crystal structures of the layered silicate nanosheets are determined, we can easily determine the framework structures of

zeolites obtained by topotactic conversion using the interlayer dehydration–condensation process. Several studies have been conducted on the synthesis of zeolites from layered silicates. CDO (the three letters indicate the framework type-code),<sup>3</sup> NSI,<sup>6</sup> CAS-NSI,<sup>7</sup> RWR,<sup>8-10</sup> RRO,<sup>11</sup> and SOD<sup>12</sup>-type zeolites were prepared using layered silicates PLS-1,<sup>3</sup> (isomorphic materials: PLS-4,<sup>13</sup> RUB-36,<sup>14,15</sup> MCM-47,<sup>16</sup> MCM-65,<sup>17</sup> UZM-13,<sup>18</sup> UZM-17,<sup>18</sup> and UZM-19<sup>18</sup>), Nu-6(1),<sup>6</sup> EU-19,<sup>7</sup> RUB-18,<sup>19,20</sup> RUB-39,<sup>21</sup> and RUB-15,<sup>22</sup> respectively. In some cases, organic cations are intercalated into the interlayer to control the layer-stacking sequence.

Formation of ordered mesoporous silica derived from layered silicates, especially kanemite, was extensively investigated by the Kuroda group.<sup>23-26</sup> They concluded that the formation of mesophase silicates from layered silicates with a single silicate sheet depends on a combination of factors, including the reactivity of the layered silicates, presence of layered intermediates, variations in the silicate sheet, and assembly of surfactant molecules in the interlayer.<sup>23-27</sup> FSM-16-type mesoporous silica is formed *via* layered intermediates composed of fragmented silicate sheets and alkyltrimethylammonium ( $\text{C}_n\text{TMA}$ ) cations. KSW-2 mesoporous silica can be prepared by bending the individual silicate sheets using intralayer and interlayer condensation. These findings indicate that the layered silicates have high potential for use in the synthesis of ordered mesoporous silica. However, only a few studies have been conducted on transformation of layered silicates, other than kanemite, into mesoporous materials.<sup>27</sup>

<sup>a</sup>Department of Applied Chemistry, Graduate School of Engineering, Hiroshima University, Higashi-Hiroshima 739-8527, Japan. E-mail: tsano@hiroshima-u.ac.jp

<sup>b</sup>Japan Fine Ceramics Center, Atsuta-ku, Nagoya 456-8587, Japan

<sup>c</sup>National Institute of Advanced Industrial Science and Technology (AIST), 4-2-1 Nigatake, Sendai 983-8551, Japan

<sup>d</sup>National Institute for Materials Science (NIMS), 1-1 Namiki, Tsukuba, Ibaraki 305-0044, Japan

† Electronic supplementary information (ESI) available: <sup>13</sup>C CP MAS NMR spectra of HUS-5 and HUS-1, and XRD patterns of HUS-1, HUS-1 ion-exchanged with 0.5 M NaCl solution, HUS-1 ion-exchanged with 0.5 M NaOH solution and HUS-5. See DOI: 10.1039/c3ta11971h

Therefore, the synthesis of novel layered silicates with unique crystal structures and their conversion to porous materials remain challenging subjects of research.

Recently, we reported the successful synthesis and structural analysis of a new layered silicate, HUS-1 ( $\text{Si}_{10}\text{O}_{24}\text{H}_8 \cdot 2(\text{CH}_3)_4\text{N}$ ).<sup>28</sup> HUS-1 consists of a half sodalite cage framework structure and a tetramethylammonium cation ( $\text{TMA}^+$ ) in the hemispherical sodalite cage, which acts as a structure-directing agent (SDA). Although the interlayer distance of HUS-1 was estimated to be approximately 0.15 nm, which was unusually short compared to those of other layered silicates, HUS-1 modified with dimethyldichlorosilane effectively and selectively adsorbed  $\text{TMA}^+$  from water, even in the presence of aqueous phenol.<sup>29</sup> Although HUS-1 was obtained by the hydrothermal treatment and then thorough washing, recently, during a further analytical study on HUS-1, we discovered that the crystal structure of the as-synthesized HUS-1 changed with the number of washings performed. The crystal structure of as-synthesized HUS-1 with 1–3 washings, named as HUS-5, was structurally similar to  $\beta$ -HLS,<sup>30</sup> whose interlayer distance was much greater than that of HUS-1 obtained by thorough washing. It is well recognized that the physicochemical properties of layered silicates are influenced by the stacking state as well as the interlayer distance of silicate layers.<sup>19,12,31</sup> This fact motivated us to investigate the difference between the respective ion-exchange behaviors of HUS-1 and HUS-5, for which they were ion-exchanged with bulky organic cations, namely dodecyltrimethylammonium ( $\text{C}_{12}\text{TMA}$ ), hexadecyltrimethylammonium ( $\text{C}_{16}\text{TMA}$ ), and benzyltrimethylammonium (BTMA). We also studied the potential of ion-exchanged layered silicates for use as base catalysts and their suitability for transformation into porous materials by post-treatment.

## Experimental

### Synthesis of HUS-5

The starting synthesis mixture was prepared using fumed silica (Cab-O-Sil M5, CABOT Co., USA), tetramethylammonium hydroxide (TMAOH, 48–50 wt%, Aldrich), sodium hydroxide (>99%, High Purity Chemical Inc., Japan), and distilled water. The resulting hydrogel, with a chemical composition of  $\text{SiO}_2 : 0.6 \text{ TMAOH} : 0.2 \text{ NaOH} : 5.5\text{H}_2\text{O}$ , was transferred to a Teflon-lined stainless steel vessel and heated under static conditions at 140 °C for 3 days. The solid product obtained (layered silicate) was separated by centrifugation and repeatedly washed with about 50 mL of distilled water. HUS-5 was obtained after 1–3 washings, whereas HUS-1 was obtained by thorough washing until the supernatant became neutral.

### Ion-exchange of HUS-1 and HUS-5

Various ion-exchange processes of HUS-1 and HUS-5 were carried out using dodecyltrimethylammonium chloride ( $\text{C}_{12}\text{TMACl}$ , Tokyo Chemical Ind. Co. Ltd., Japan), hexadecyltrimethylammonium chloride ( $\text{C}_{16}\text{TMACl}$ , Tokyo Chemical Ind. Co. Ltd., Japan), and benzyltrimethylammonium chloride (BTMACl, Tokyo Chemical Ind. Co. Ltd., Japan) as

alkylammonium surfactants. The layered silicate (0.1 g) was dispersed in an aqueous solution (20 mL) of alkylammonium chloride (1.1 mmol). The mixture was stirred at room temperature for 0.5 h and then centrifuged to remove the supernatant. This procedure was repeated three times.

### Catalytic test

The Knoevenagel condensation reaction, which is used as a test reaction for a base catalyst, was carried out as follows. A mixture of benzaldehyde (4.0 mmol), ethyl cyanoacetate (3.5 mmol), and naphthalene (0.35 mmol, as an internal standard) in ethanol (3 mL) was added to a flask containing the layered silicate (HUS-1 or HUS-5 ion-exchanged with organic surfactants) as a catalyst (25 mg). The reaction was carried out at room temperature under stirring. After filtration of the solid, the filtrate was analyzed using a GC equipped with an FID-type detector on a Zebtron ZB-1 column to determine the conversion of ethyl cyanoacetate and product yield.

### Transformation of ion-exchanged HUS-5 into porous silica

Transformation of HUS-5, ion-exchanged with various alkylammonium cations, into a porous material was carried out by acid treatment, followed by calcination. The alkylammonium ion-exchanged HUS-5 (200 mg) was dispersed in distilled water (20 mL), and then 1.0 M acetic acid aqueous solution was added dropwise to the mixture to adjust the pH value between 2.5 and 5.5. The resulting mixture was then stirred at room temperature for 1 day. Next, the obtained solid product was separated by filtration, dried at 70 °C, and then calcined at 550 °C for 6 h to completely remove organic fractions.

### Characterization

Powder X-ray diffraction (XRD) patterns of the solid products were collected using a powder X-ray diffractometer (Rigaku, Mini Flex) with graphite-monochromatized Cu K $\alpha$  radiation at 30 kV and 15 mA. Crystal morphology and elemental composition were determined using a Hitachi S-4800 scanning electron microscope (SEM) coupled to an energy-dispersive X-ray (EDX) analyzer. <sup>29</sup>Si MAS NMR spectra were recorded at 119.17 MHz on a Varian 600PS solid NMR spectrometer using a 6 mm diameter zirconia rotor. The rotor was spun at 7 kHz. The spectra were acquired using 6.7  $\mu$ s pulses, a 100 s recycle delay, and 1000 scans. 3-(Trimethylsilyl)propionic-2,2,3,3-d<sub>4</sub> acid sodium salt was used as a chemical shift reference. <sup>1</sup>H MAS NMR spectra were measured using a spinning frequency of 20 kHz and a single pulse sequence operated at 599.85 MHz using a 3.2 mm diameter zirconia rotor. Furthermore, <sup>1</sup>H-<sup>13</sup>C CP MAS NMR spectra were also measured with a spinning frequency of 20 kHz, a 90° pulse length of 2.2  $\mu$ s, and a cycle delay time of 100 s using a 3.2 mm diameter zirconia rotor. The <sup>1</sup>H and <sup>13</sup>C chemical shifts were referenced to adamantane and hexamethylbenzene, respectively. Nitrogen adsorption–desorption isotherms were obtained at –196 °C using a conventional volumetric apparatus (Bel Japan, BELSORP-mini). Prior to the adsorption measurements, the samples (*ca.* 0.1 g) were evacuated at 200 °C for 3 h. Thermal analyses were carried out using a

TG/DTA apparatus (SSC/5200, Seiko Instruments). A sample (*ca.* 3 mg) was heated in a flow of air ( $50 \text{ mL min}^{-1}$ ) at a heating rate of  $10 \text{ }^\circ\text{C min}^{-1}$  from room temperature to  $800 \text{ }^\circ\text{C}$ . Elemental analysis was carried out using a Perkin-Elmer 2400II CHN analyzer at the Natural Science Center for Basic Research and Development (N-BARD), Hiroshima University. Transmission electron microscopy (TEM) images of nanoporous silica were taken using a Hitachi H9500 microscope at an acceleration voltage of 300 kV. IR spectra were recorded using an FT-IR spectrometer (NICOLET 6700) with a resolution of  $4 \text{ cm}^{-1}$  at room temperature. The sample was first pressed into a self-supporting thin wafer (*ca.*  $10 \text{ mg cm}^{-2}$ ), and then placed into a quartz IR cell equipped with  $\text{CaF}_2$  windows.

## Results and discussion

### Synthesis and characteristics of HUS-5

Fig. 1(A) shows the XRD patterns of the as-synthesized layered silicates. When the number of washings was  $<2$ , the peaks assigned to HUS-1 were not observed, indicating the formation of another type of layered silicate with a different crystal structure, which was named HUS-5. After 3 washings, diffraction peaks that correspond to HUS-1 phase became observable and the peak intensities increased with washing. The product obtained after 10 washings had the well-defined HUS-1 structure.<sup>28</sup> The basal spacing of HUS-5 ( $d = 1.13 \text{ nm}$ ,  $2\theta = 7.8^\circ$ ) was greater than that of HUS-1 ( $d = 0.89 \text{ nm}$ ,  $2\theta = 9.9^\circ$ ). Fig. 1(B) shows the relationship between the peak intensities at  $7.8^\circ$  and  $9.9^\circ$  and the number of  $\text{Na}^+$  cations per unit cell. The amounts of  $\text{Na}^+$  cations in the products were determined by SEM/EDX. The peak intensity at  $7.8^\circ$  decreased with a decrease in the number of  $\text{Na}^+$  cations, whereas the peak intensity at  $9.9^\circ$  increased with a decrease in the number of  $\text{Na}^+$  cations. This observation strongly indicates that  $\text{Na}^+$  cations were substituted with protons and de-intercalated from the interlayer during washing. Fig. 2 shows the SEM images of HUS-5 and HUS-1. There are no differences in the morphology (square, plate-like) and particle sizes ( $0.8 \times 1.2 \text{ }\mu\text{m}$ ) between HUS-1 and HUS-5, indicating that the crystal structure was retained after washing.

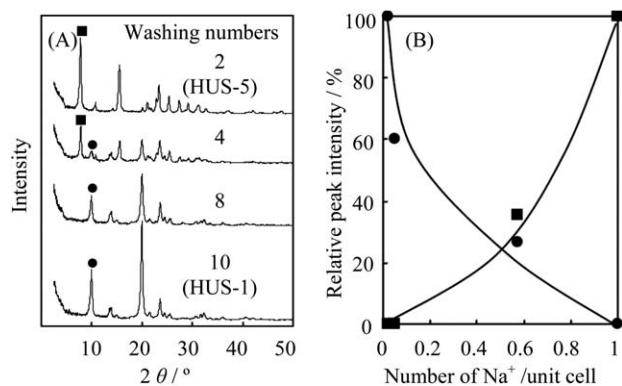


Fig. 1 (A) XRD patterns of as-synthesized HUS-1 obtained with different washing numbers and (B) relationship between relative peak intensities of (■)  $2\theta = 7.8^\circ$  (HUS-5) and (●)  $2\theta = 9.9^\circ$  (HUS-1) and the number of  $\text{Na}^+$  in the unit cell.

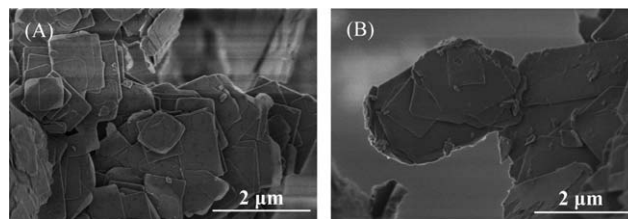


Fig. 2 SEM images of (A) HUS-5 and (B) HUS-1.

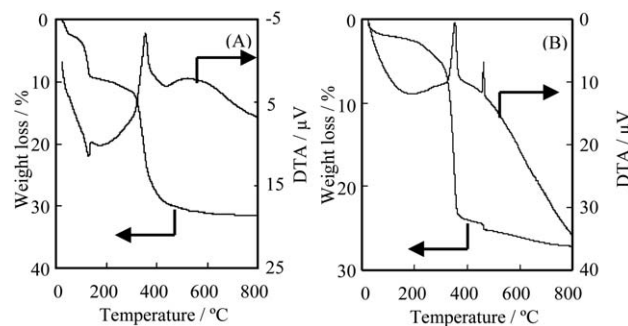


Fig. 3 TG-DTA curves of (A) HUS-5 and (B) HUS-1.

In the  $^{13}\text{C}$  CP MAS NMR spectra of both HUS-5 and HUS-1, a sharp resonance peak centered at *ca.* 58 ppm was observed (Fig. S1†). The peak can be assigned to methyl groups attached to N, namely the  $\text{CH}_3$  moiety of  $\text{N-CH}_3$ . Therefore,  $\text{TMA}^+$  was the only organic species present in HUS-1 and HUS-5. To quantify the amount of  $\text{TMA}^+$  present, TG/DTA measurements were performed. As presented in Fig. 3, the thermal profiles can be categorized into three temperature zones: (I)  $25\text{--}250 \text{ }^\circ\text{C}$ , (II)  $250\text{--}350 \text{ }^\circ\text{C}$ , and (III)  $350\text{--}700 \text{ }^\circ\text{C}$ . The first zone has an endothermic profile due to desorption of water. Approximately 11% weight loss is observed for HUS-5, whereas there is negligible mass loss observed for HUS-1. Thus, apparently, the interlayer of HUS-5 is more hydrophilic, compared with that of HUS-1. The second zone has an exothermic profile that can probably be attributed to the decomposition/oxidation of  $\text{TMA}^+$  that interacts with  $\text{SiOH/SiO}^-$  groups. The third zone, with an exothermic profile, could be assigned to further oxidation of carbonaceous materials generated by the decomposition of  $\text{TMA}^+$ . Although we could not assign the sharp exothermic peak at  $450 \text{ }^\circ\text{C}$  at the present time, the mass losses between 250 and  $700 \text{ }^\circ\text{C}$  for HUS-1 and HUS-5 were approximately 21 and 23 wt%, respectively, indicating no significant release of  $\text{TMA}^+$  from the interlayers during washing.

Fig. 4(A) shows the  $^{29}\text{Si}$  MAS NMR spectra of HUS-5 and HUS-1. In the spectrum of HUS-1, four resonance peaks are clearly observed, of which three at  $-102$ ,  $-105$ , and  $-107 \text{ ppm}$  may be assigned to the  $\text{Q}^3[(-\text{SiO})_3\text{Si-OH}]$  structure, whereas the fourth at *ca.*  $-114 \text{ ppm}$  may be assigned to the  $\text{Q}^4[(-\text{SiO})_4\text{Si}]$  structure.<sup>28</sup> In contrast, in the case of HUS-5, only two peaks are observed at *ca.*  $-104$  and  $-114 \text{ ppm}$ , which are because of  $\text{Q}^3$  and  $\text{Q}^4$  structures, respectively. The  $\text{Q}^3/\text{Q}^4$  ratio (83/17) of HUS-5 was consistent with that of HUS-1 (81/19), indicating that the silicate sheet structure was retained during the washing treatment. Therefore, the change in the spectrum could probably be

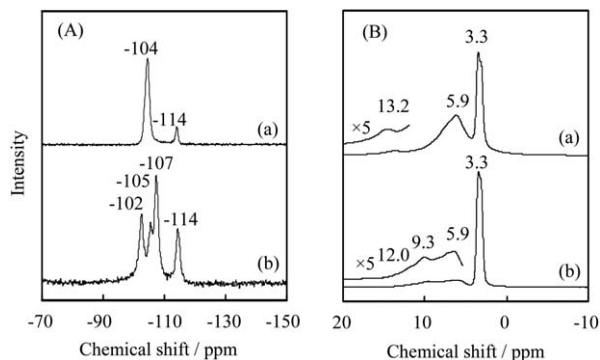


Fig. 4 (A)  $^{29}\text{Si}$  and (B)  $^1\text{H}$  MAS NMR spectra of (a) HUS-5 and (b) HUS-1.

attributed to the presence of  $\text{Na}^+$  cations and hydrated water in the interlayers of HUS-5. To investigate the configuration of silanol groups,  $^1\text{H}$  MAS NMR measurements were performed. Fig. 4(B) shows the  $^1\text{H}$  MAS NMR spectra of HUS-1 and HUS-5. The sharp and broad peaks at 3.3 and 5.9 ppm may be assigned to the protons of the methyl groups of  $\text{TMA}^+$  cations and to adsorbed hydrogen-bonded water molecules ( $\text{SiOH}\cdots\text{H}_2\text{O}$  or  $\text{H}_2\text{O}\cdots\text{H}_2\text{O}$ ), respectively. The broad peaks at 9.3, 12.0, and 13.2 ppm are attributed to silanol groups with strong hydrogen bonding ( $\text{SiOH}\cdots\text{OSi}$ ). These NMR results suggest that strong hydrogen bonding exists between the silanol groups on both sides of the interlayer, as well as between the vicinal silanols in the intralayer of both HUS-5 and HUS-1.

Taking into account the data obtained by CHN elemental analysis and EDX, together with the above results, the chemical composition of HUS-5 was estimated to be  $\text{Si}_{10}\text{O}_{24}\text{H}_5\cdot 1.9[(\text{CH}_3)_4\text{N}]\cdot 1.0\text{Na}\cdot 4.5\text{H}_2\text{O}$ . Furthermore, from the structural analysis obtained by powder XRD, it can be seen that the structure-type of HUS-5 is similar to that of  $\beta$ -HLS; in particular, HUS-5 had  $\text{Na}^+$ ,  $\text{TMA}^+$ , and hydrated water in the interlayer.<sup>30</sup> The stacking sequence of the neighboring layers in HUS-1 is entirely different from that in HUS-5. However, their framework topologies are similar to each other. This shows that HUS-5, with ABAB stacking order, converts to HUS-1, with AAAA stacking order, because of washing. To obtain further information concerning the structural transformation process, the following ion-exchange experiments were conducted. When HUS-1 was ion-exchanged using 0.5 M NaCl aqueous solution, there was no change in the XRD patterns of HUS-1 before and after ion-exchange (Fig. S2<sup>†</sup>). In contrast, HUS-1 was completely transformed into HUS-5 when the ion-exchange was carried out under an alkaline condition using 0.5 M NaOH aqueous solution. These results strongly suggest that the transformation of HUS-1 into HUS-5 occurs by ion-exchange of protons from silanol groups in the interlayers of HUS-1 with  $\text{Na}^+$  cations, which is activated at basic pH. Lastly, the transformation between HUS-5 and HUS-1 is a reversible process. Fig. 5 shows crystal structure models of HUS-5 and HUS-1.

#### Ion-exchange behavior of HUS-1 and HUS-5

As described above, the interlayer distance of HUS-5 was greater than that of HUS-1 because of the presence of both  $\text{Na}^+$  cations

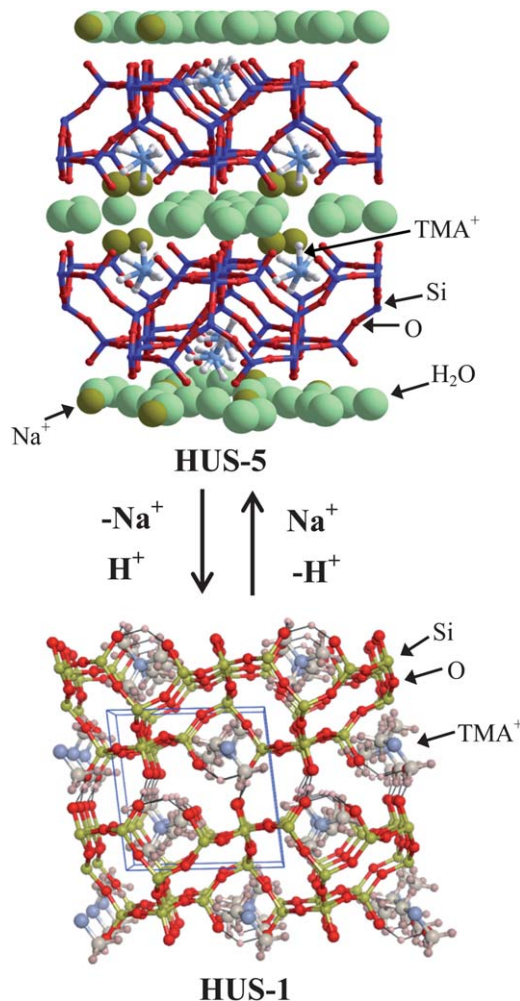
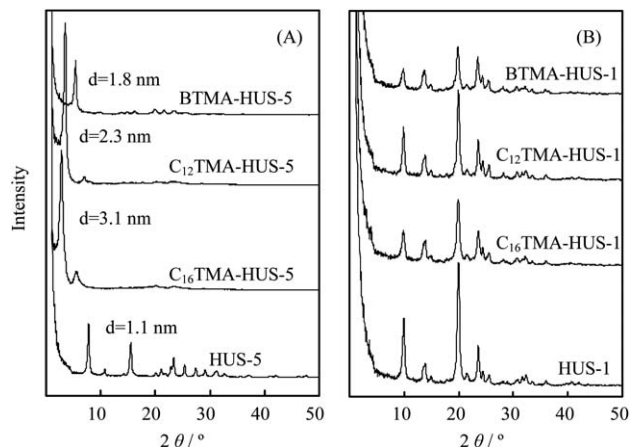
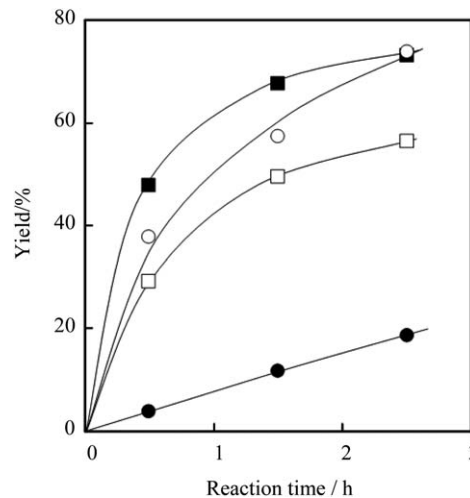


Fig. 5 Crystal structure models of HUS-5 and HUS-1.

and hydrated water in the interlayers. This suggests the possibility of further expansion of the interlayers by ion-exchange of  $\text{TMA}^+$  and  $\text{Na}^+$  cations in the interlayer with bulky organic cations. Therefore, HUS-5 was ion-exchanged in three separate samples with  $\text{C}_{12}\text{TMA}^+$ ,  $\text{C}_{16}\text{TMA}^+$  and  $\text{BTMA}^+$ , all of which are quaternary ammonium cations. For comparison, HUS-1 was also ion-exchanged with these cations. Fig. 6(A) shows the XRD patterns of HUS-5 ion-exchanged with  $\text{C}_{12}\text{TMA}^+$  ( $\text{C}_{12}\text{TMA}$ -HUS-5),  $\text{C}_{16}\text{TMA}^+$  ( $\text{C}_{16}\text{TMA}$ -HUS-5), and  $\text{BTMA}^+$  ( $\text{BTMA}$ -HUS-5). The interlayer distance of HUS-5 increased to 1.65, 2.35, and 0.85 nm for  $\text{C}_{12}\text{TMA}$ -HUS-5,  $\text{C}_{16}\text{TMA}$ -HUS-5, and  $\text{BTMA}$ -HUS-5, respectively. In contrast, (Fig. 6(B)), there were no differences in the XRD patterns of HUS-1 recorded before and after ion-exchange, suggesting that the alkylammonium cations were not intercalated in the interlayer of HUS-1. Fig. 7 shows the  $^{13}\text{C}$  CP/MAS NMR spectra of  $\text{C}_{12}\text{TMA}$ -HUS-5,  $\text{C}_{16}\text{TMA}$ -HUS-5, and  $\text{BTMA}$ -HUS-5. In addition to the  $\text{TMA}^+$  cation, the presence of  $\text{C}_n\text{TMA}$  cations was confirmed in these spectra. Based on the results of TG/DTA and elemental analysis, the chemical compositions of  $\text{C}_{12}\text{TMA}$ -HUS-5,  $\text{C}_{16}\text{TMA}$ -HUS-5, and  $\text{BTMA}$ -HUS-5 were estimated to be  $\text{Si}_{10}\text{O}_{24}\text{H}_6\cdot 0.5[\text{TMA}]\cdot 1.5[\text{C}_{12}\text{TMA}]$ ,  $\text{Si}_{10}\text{O}_{24}\text{H}_{5.7}\cdot 0.4[\text{TMA}]\cdot 1.9[\text{C}_{16}\text{TMA}]$ , and  $\text{Si}_{10}\text{O}_{24}\text{H}_6\cdot 0.7[\text{TMA}]\cdot$



**Fig. 6** XRD patterns of (A) HUS-5 and (B) HUS-1 ion-exchanged with various quaternary alkylammonium cations.



**Fig. 8** Knoevenagel reaction over (●) HUS-1, (○) BTMA-HUS-5, (■) C<sub>12</sub>TMA-HUS-5, and (□) C<sub>16</sub>TMA-HUS-5.

1.3[BTMA], respectively. Moreover, it was found that the expansion of the interlayer spacing of HUS-5 was due to the ion-exchange of Na<sup>+</sup> cations, and some TMA<sup>+</sup> cations in the interlayer, with these bulky ammonium cations. Furthermore, as Na<sup>+</sup> cations were not detected in the ion-exchanged HUS-5, it is thought that several SiO<sup>-</sup> groups were protonated and converted to SiOH.

Recently, the layered silicate PLS-1, which possesses TMAOH in the interlayers, was found to exhibit catalytic activity when used in a Knoevenagel condensation reaction as a base catalyst. The latter reaction is a fundamental means of encouraging C-C bond formation.<sup>33</sup> However, there are few reports concerning the catalytic activity of layered silicates, other than PLS-1, or the literature on the effect of the interlayer expansion of layered silicates on the catalytic performance in the Knoevenagel condensation. Therefore, in order to clarify the respective potentials of C<sub>12</sub>TMA-HUS-5, C<sub>16</sub>TMA-HUS-5, and BTMA-HUS-5 for use as base catalysts, the Knoevenagel condensation reaction of benzaldehyde with ethyl cyanoacetate was investigated. For comparison, the catalytic performance of HUS-1 was

also evaluated. The reaction occurred quantitatively, even at room temperature (25 °C), to yield the product (ethyl-2-cyano-3-phenylacrylate) with a selectivity of >95%. Fig. 8 shows the results of the Knoevenagel condensation reaction over these catalysts. The respective catalytic activities of C<sub>12</sub>TMA-HUS-5, C<sub>16</sub>TMA-HUS-5, and BTMA-HUS-5 are considerably higher than that of HUS-1. These high catalytic performances were probably due to large interlayer spacings that facilitated easier diffusion of reagents and products. The difference in the respective catalytic activities of C<sub>12</sub>TMA-HUS-5, C<sub>16</sub>TMA-HUS-5, and BTMA-HUS-5 seems to be because of the difference in diffusion limitation between reagents and products. Furthermore, the catalytic performance was much higher as compared with other types of layered silicates such as HUS-2, HUS-3 and PLS-1.<sup>32,33</sup>

#### Conversion of HUS-5, ion-exchanged with alkylammonium cations, into porous silica

Alkylammonium-layered silicate complexes have been used as precursors of mesoporous silica.<sup>23-26</sup> Kimura *et al.* reported the

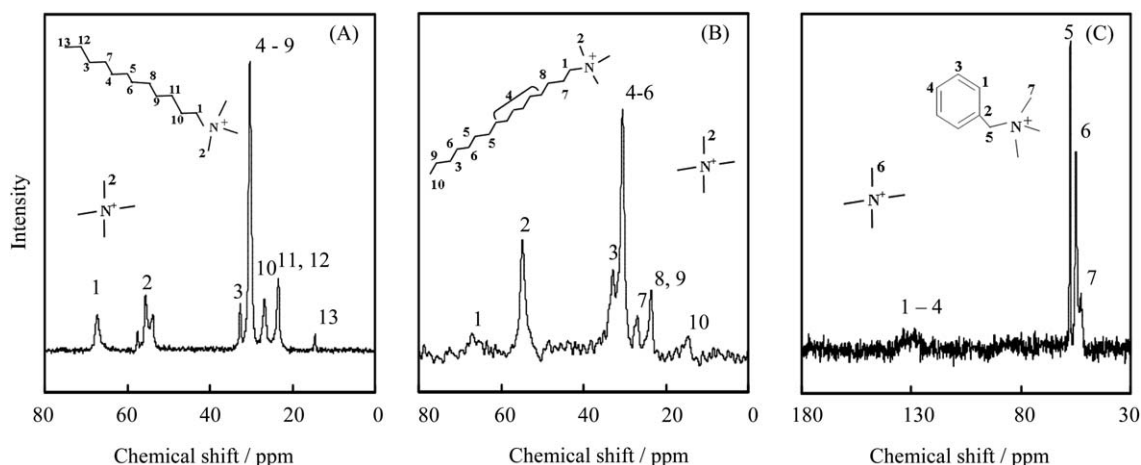


**Fig. 7** <sup>13</sup>C CP/MAS NMR spectra of (A) C<sub>12</sub>TMA-HUS-5, (B) C<sub>16</sub>TMA-HUS-5, and (C) BTMA-HUS-5.

**Table 1** Characteristics of the HUS-5 ion-exchanged with various alkylammonium cations after acid treatment followed by calcination at 550 °C for 6 h

Sample no.	Acid treatment condition				BET surface area <sup>a</sup> /m <sup>2</sup> g <sup>-1</sup>	Pore diameter <sup>b</sup> /nm
	Alkylammonium cation	pH value	Temperature/°C	Time/h		
1	C <sub>16</sub> TMA				200	
2	C <sub>16</sub> TMA	5.5	25	24	440	
3	C <sub>16</sub> TMA	4.5	25	24	780	1.28
4	C <sub>16</sub> TMA	2.5	25	24	983	1.62
5	C <sub>12</sub> TMA	2.5	25	24	165	
6	BTMA	2.5	25	24	209	

<sup>a</sup> Determined by the BET method. <sup>b</sup> Determined by the BJH plot.

formation of KSW-2 with square and lozenge one-dimensional (1D) by mild acid treatment of a layered alkylammonium-kanemite complex.<sup>26</sup> In previous work, we also succeeded in the preparation of a microporous material, which had an average pore diameter of 0.55 nm, from intermediates.<sup>34</sup> The latter were obtained by the intercalation of acetic acid molecules and TMA<sup>+</sup> cations into the interlayer of layered silicate magadiite and converted to the microporous material through the dehydration-condensation of silanol groups on both sides of the interlayer. It became clear that the control of both the stacking sequence and the configuration of the silanol groups, on both sides of the interlayer, are important factors for the zeolitization of layered silicates. Although the layered framework structure of HUS-1 is more complicated than those of kanemite and magadiite, these facts motivated us to use alkylammonium-HUS-5 complexes as precursors for porous materials. The HUS-5, which contained TMA<sup>+</sup> cations in the interlayer, was thermally treated at 550 °C. However, only broad and hollow peaks, corresponding to amorphous materials, were observed in the XRD pattern, indicating the degradation of the layered structure of HUS-5; probably, the state of the silicate layers, such as the stacking sequence, was not suitable for formation of the porous

material. Therefore, we attempted to convert HUS-5, ion-exchanged with alkylammonium cations, to a porous material by a multi-stage process that involved acid treatment and subsequent calcination.

Typical treatment conditions and characteristics of the products obtained are listed in Table 1. When C<sub>16</sub>TMA-HUS-5 was calcined at 550 °C for 6 h (sample no. 1), the product had a BET surface area of 200 m<sup>2</sup> g<sup>-1</sup>. However, when C<sub>16</sub>TMA-HUS-5 was treated in acetic acid aqueous solutions with various pH values, considerable increases in BET surface areas were observed, especially at a pH value of 2.5 (sample no. 4), which was named HUS-6. The N<sub>2</sub> adsorption-desorption isotherms of HUS-6 are shown in Fig. 9. The pore size distribution, calculated from the adsorption branch, is also shown. The BET surface area, pore volume, and average pore diameter of the HUS-6 were calculated to be 983 m<sup>2</sup> g<sup>-1</sup>, 0.45 cm<sup>3</sup> g<sup>-1</sup>, and 1.62 nm, respectively. The N<sub>2</sub> adsorption isotherm exhibited a steep increase in the N<sub>2</sub> adsorption amount at low relative pressure; this suggests the existence of nanopores. Fig. 10(a) shows the XRD pattern of the HUS-6 (sample no. 4). Although no peaks are observed in the range 2θ = 10–50°, a broad peak is seen at ca. 2.9°, corresponding to a basal spacing of 3.02 nm, indicating regulation of pore formation in the HUS-6. Fig. 11 shows the

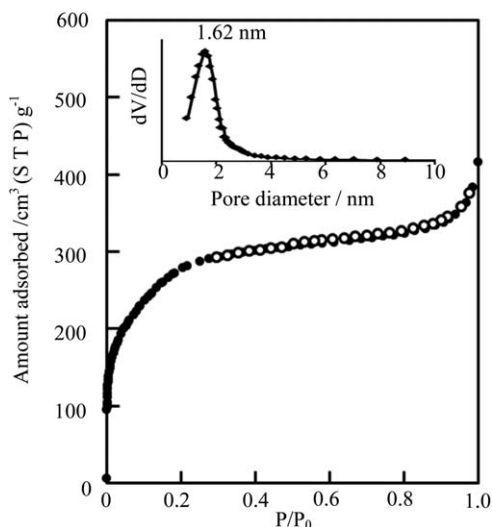


**Fig. 9** N<sub>2</sub> adsorption (●)–desorption (○) isotherms and pore size distribution of HUS-6 (sample no. 4).

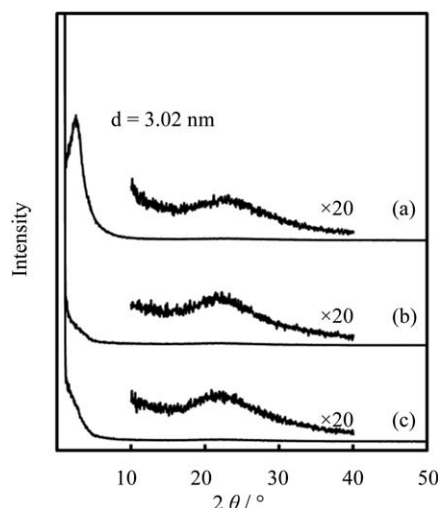


**Fig. 10** XRD patterns of (a) HUS-6 (sample no. 4), (b) sample no. 5, and (c) sample no. 6.

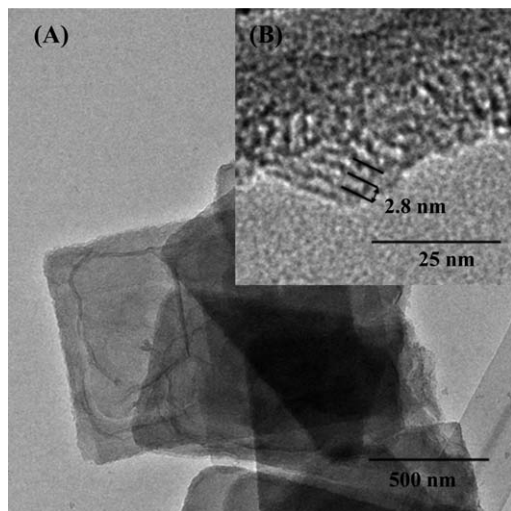


Fig. 11 TEM images of HUS-6 (sample no. 4).

TEM images of the HUS-6. The slightly disordered nanopores with a pore size range of 1.0–2.0 nm are clearly observed. The periodic distance of adjacent pores (*ca.* 2.8 nm) was in agreement with the basal *d*-spacing of HUS-6 (3.02 nm). It was also found that no morphology change occurred after the acid and calcination treatments, which indicated that there was no dissolution of silicate layers during the post-treatment involved acid treatment and subsequent calcination. Although the post-treatment of C<sub>12</sub>TMA-HUS-5 and BTMA-HUS-5 was also carried out, no significant formation of ordered nanopores was observed in XRD patterns (Fig. 10(b) and (c)).

To obtain further information concerning the formation process of HUS-6, <sup>29</sup>Si MAS NMR spectra were obtained (Fig. 12). The latter shows the following spectra: C<sub>16</sub>TMA-HUS-5,

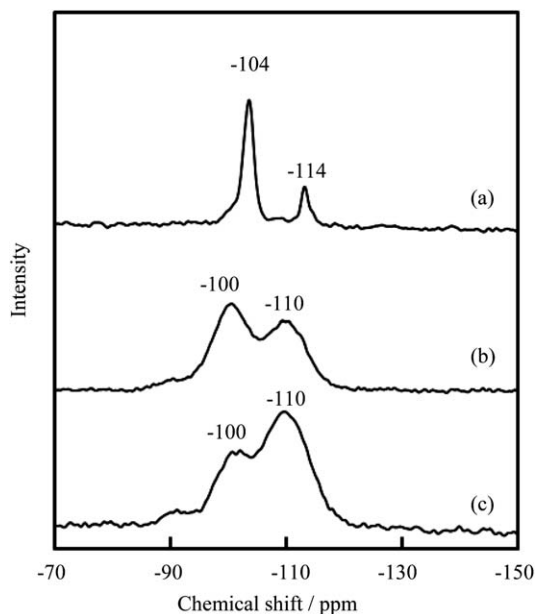


Fig. 12 <sup>29</sup>Si MAS NMR spectra of (a) C<sub>16</sub>TMA-HUS-5, (b) C<sub>16</sub>TMA-HUS-5 after only acetic acid treatment (no calcination), and (c) C<sub>16</sub>TMA-HUS-5 after acetic acid treatment and subsequent calcination (HUS-6).

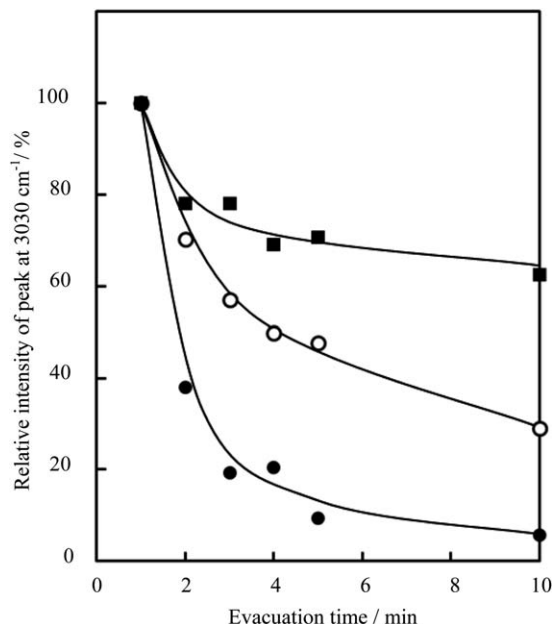


Fig. 13 Relationship between relative intensity of the peak at 3030 cm<sup>-1</sup> and evacuation time on (O) HUS-6, (●) MCM-41, and (■) silicalite-1.

C<sub>16</sub>TMA-HUS-5 after acetic acid treatment only, and C<sub>16</sub>TMA-HUS-5 after both acid treatment and subsequent calcination (HUS-6). In the spectrum of C<sub>16</sub>TMA-HUS-5, only two peaks are observed at *ca.* -104 and -114 ppm, which are assigned to Q<sup>3</sup> and Q<sup>4</sup> structures, respectively. As the spectrum was consistent with that of the as-synthesized HUS-5, it was found that the framework structure of HUS-5 was retained during the ion-exchange. In contrast, the profile of C<sub>16</sub>TMA-HUS-5 after acid treatment was different to that of C<sub>16</sub>TMA-HUS-5. The latter showed broad Q<sup>3</sup> and Q<sup>4</sup> peaks at -100 and -110 ppm, respectively. The Q<sup>3</sup>/Q<sup>4</sup> ratio of C<sub>16</sub>TMA-HUS-5 after acid treatment was 59/41. Furthermore, this value for HUS-6 changed to 38/62. This strongly indicates that the dehydration-condensation of silanol groups in the interlayer or intralayer occurred by acid treatment and subsequent calcination.<sup>26</sup> Moreover, since the Q<sup>2</sup> peak was not observed, the cleavage of Si-O-Si bonds in the framework was negligible, so that, essentially, the framework structure of the silicate sheets was retained after the acid treatment and calcination.<sup>35</sup> However, there is room for examination of the exact formation mechanism of the nanopores in HUS-6 at the present time, and we are conducting further investigation on the transformation.

As stated above, the pore size of the HUS-6 obtained was smaller than that of MCM-41 (*ca.* 2.9 nm), which was synthesized using hexadecyltrimethylammonium bromide. To our knowledge, there are few reports concerning the preparation of ordered nanoporous silica with a pore size of 1–2 nm,<sup>36</sup> which indicates that the HUS-6 with its unique pore structure can be used as a shape-selective catalyst and adsorbent. In order to determine any influence of pore size on the adsorption-desorption behavior of porous silica, we investigated the desorption behavior of toluene on HUS-6. MCM-41 (*ca.* 2.9 nm) as mesoporous silica and silicalite-1 (*ca.* 0.6 nm) as MFI type

pure silica zeolite were used as references. These samples were evacuated at 400 °C for 3 h, and then adsorption of toluene was carried out at 25 °C for 1 h. Afterwards, samples were evacuated at room temperature for various times, and then the samples' FT-IR spectra were measured to evaluate the amount of the remaining toluene. Fig. 13 shows the relationship between the intensity of the peak at *ca.* 3030 cm<sup>-1</sup> that is assigned to the C–H stretching vibration of the toluene molecule and the evacuation time for HUS-6, MCM-41, and silicalite-1. For MCM-41, the peak intensity decreases rapidly with evacuation time, suggesting that toluene molecules had been weakly adsorbed in the mesopores of MCM-41. On the other hand, for silicalite-1, approximately 63% of toluene molecules were still present even after 10 min evacuation. In the case of HUS-6, approximately 29% of toluene molecules remained in the nanopores after 10 min evacuation. These results strongly indicate that nanopores of HUS-6 present a unique adsorption space when compared with both micropores (*ca.* 0.6 nm) of silicalite-1 and mesopores (*ca.* 2.9 nm) of MCM-41.

## Conclusions

We prepared the HUS-1 precursor, HUS-5, whose crystal structure was similar to that of β-HLS layered silicate. The interlayer distance of HUS-5 was 0.4 nm, and TMA<sup>+</sup>, Na<sup>+</sup>, and hydrated water were present in the interlayer. HUS-5 with ABAB stacking order was converted to HUS-1 with AAAA stacking order during washing treatment. An increase in the interlayer distance of HUS-5 was observed when the latter was ion-exchanged with bulky organic cations such as dodecyltrimethylammonium, hexadecyltrimethylammonium, and benzyltrimethylammonium. In addition, HUS-5, ion-exchanged with any of the several organic cations tested, could be employed as a base catalyst. Also, the alkylammonium ion-exchanged HUS-5 variants exhibited high catalytic activities in Knoevenagel condensation reactions.

Separately, we also succeeded in the conversion of HUS-5, ion-exchanged with hexadecyltrimethylammonium cations, to novel nanoporous silica (HUS-6) by an acetic acid treatment and subsequent calcination. The BET surface area, pore volume, and average pore diameter of HUS-6 were 983 m<sup>2</sup> g<sup>-1</sup>, 0.45 cm<sup>3</sup> g<sup>-1</sup>, and 1.62 nm, respectively. In order to determine any influence of pore size on the adsorption properties of porous silica with different pore sizes, desorption experiments were performed for HUS-6, MCM-41, and silicalite-1. The adsorption–desorption behavior of toluene on HUS-6 showed that there was an intermediate state between MCM-41 and silicalite-1. Therefore, it was found that nanopores (mean size *ca.* 1.6 nm) of HUS-6 present a unique adsorption space as compared to micropores (mean size *ca.* 0.6 nm) of silicalite and mesopores (mean size *ca.* 2.9 nm) of MCM-41.

## Notes and references

- N. Takahashi and K. Kuroda, *J. Mater. Chem.*, 2011, **21**, 14336.
- (a) M. Ogawa and K. Kuroda, *Bull. Chem. Soc. Jpn.*, 1997, **70**, 2593; (b) T. Okada, Y. Ide and M. Ogawa, *Chem.–Asian J.*, 2012, **7**, 1980.
- T. Ikeda, Y. Akiyama, Y. Oumi, A. Kawai and F. Mizukami, *Angew. Chem., Int. Ed.*, 2004, **43**, 4892.
- B. Marler and H. Gies, *Eur. J. Mineral.*, 2012, **24**, 405.
- T. Kimura and K. Kuroda, *Adv. Funct. Mater.*, 2009, **19**, 511.
- S. Zanardi, A. Alberti, G. Cruciani, A. Corma, V. Fornes and M. Brunelli, *Angew. Chem., Int. Ed.*, 2004, **43**, 4933.
- B. Marler, M. A. Camblor and H. Gies, *Microporous Mesoporous Mater.*, 2006, **90**, 87.
- B. Marler, N. Stroter and H. Gies, *Microporous Mesoporous Mater.*, 2005, **83**, 201.
- Y. Oumi, T. Takeoka, T. Ikeda, T. Yokoyama and T. Sano, *New J. Chem.*, 2007, **31**, 593.
- T. Ikeda, Y. Oumi, T. Takeoka, T. Yokoyama, T. Sano and T. Hanaoka, *Microporous Mesoporous Mater.*, 2008, **110**, 488.
- Y. Wang, B. Marler, H. Gies and U. Muller, *Chem. Mater.*, 2005, **17**, 43.
- T. Moteki, W. Chaikiiisilp, A. Shimojima and T. Okubo, *J. Am. Chem. Soc.*, 2008, **130**, 15780.
- T. Ikeda, S. Kayamori and F. Mizukami, *J. Mater. Chem.*, 2009, **19**, 5518.
- J. Song and H. Gies, *Stud. Surf. Sci. Catal.*, 2004, **154A**, 295.
- B. Marler, Y. Wang, H. Song and H. Gies, *Abstracts of Papers, 15<sup>th</sup> International Zeolite Conference, 2007*, Beijing, China, August 12–17, 2007, p. 599.
- A. Burton, R. J. Accardi, R. F. Lobo, M. Falcioni and M. W. Deem, *Chem. Mater.*, 2000, **12**, 2936.
- D. L. Dorset and G. J. Kennedy, *J. Phys. Chem. B*, 2004, **108**, 15216.
- L. M. Knight, M. A. Miller, S. C. Koster, M. G. Gatter, A. I. Benin, R. R. Willis, G. J. Lewis and R. W. Broach, *Stud. Surf. Sci. Catal.*, 2007, **170A**, 338.
- A. J. Blake, K. R. Franklin and B. M. Lowe, *J. Chem. Soc., Dalton Trans.*, 1988, 2513.
- S. Vortmann, J. Rius, S. Siegmann and H. Gies, *J. Phys. Chem. B*, 1997, **101**, 1292.
- Y. X. Wang, H. Gies and J. H. Lin, *Chem. Mater.*, 2007, **19**, 4181.
- U. Oberhagemann, P. Bayat, B. Marler, H. Gies and J. Rius, *Angew. Chem., Int. Ed.*, 1996, **35**, 2869.
- T. Yanagisawa, T. Shimizu, K. Kuroda and C. Kato, *Bull. Chem. Soc. Jpn.*, 1990, **63**, 988.
- S. Inagaki, Y. Fukushima and K. Kuroda, *J. Chem. Soc., Chem. Commun.*, 1993, 680.
- S. Inagaki, A. Koiwai, N. Suzuki, Y. Fukushima and K. Kuroda, *Bull. Chem. Soc. Jpn.*, 1996, **69**, 1449.
- T. Kimura, T. Kamata, M. Fuziwarra, Y. Takano, M. Kaneda, Y. Sakamoto, O. Terasaki, Y. Sugahara and K. Kuroda, *Angew. Chem., Int. Ed.*, 2000, **39**, 3855.
- R. García, I. Díaz, C. Márquez-Álvarez and J. Pérez-Pariente, *Chem. Mater.*, 2006, **18**, 2283.
- T. Ikeda, Y. Oumi, K. Honda, T. Sano, K. Momma and F. Izumi, *Inorg. Chem.*, 2011, **50**, 2294.
- Y. Ide, M. Torii, N. Tsunoji, M. Sadakane and T. Sano, *Chem. Commun.*, 2012, **48**, 7073.
- T. Ikeda, Y. Akiyama, F. Izumi, Y. Kiyozumi, F. Mizukami and T. Kodaira, *Chem. Mater.*, 2001, **13**, 1286.

- 31 N. Tsunoji, Y. Ide, M. Torii, M. Sadakane and T. Sano, *Chem. Lett.*, 2013, **42**, 244.
- 32 N. Tsunoji, T. Ikeda, Y. Ide, M. Sadakane and T. Sano, *J. Mater. Chem.*, 2012, **22**, 13682.
- 33 K. Komura, T. Kawakami and Y. Sugi, *Catal. Commun.*, 2007, **8**, 644.
- 34 Y. Oumi, K. Takagi, T. Ikeda, H. Sasaki, T. Yokoyama and T. Sano, *J. Porous Mater.*, 2009, **16**, 641.
- 35 L. Liebau, *Structural Chemistry of Silicates*, Springer, Heidelberg, 1985.
- 36 M. J. Kim and R. Ryoo, *Chem. Mater.*, 1999, **11**, 487–491.